1-1-2013

Ro-vibrational Quenching of CO ($v = 1$) by He Impact in a Broad Range of Temperatures: A Benchmark Study Using Mixed Quantum/Classical Inelastic Scattering Theory

Alexander Semenov
Marquette University

Mikhail V. Ivanov
Marquette University

Dmitri Babikov
Marquette University, dmitri.babikov@marquette.edu

Published version. *Journal of Chemical Physics*, Vol. 139 (2013): 074306: 1-12. DOI.

Ro-vibrational quenching of CO ($v = 1$) by He impact in a broad range of temperatures: A benchmark study using mixed quantum/classical inelastic scattering theory

Alexander Semenov, Mikhail Ivanov, and Dmitri Babikov[a)]
Chemistry Department, Wehr Chemistry Building, Marquette University, Milwaukee, Wisconsin 53201-1881, USA

(Received 25 June 2013; accepted 31 July 2013; published online 20 August 2013)

The mixed quantum/classical approach is applied to the problem of ro-vibrational energy transfer in the inelastic collisions of CO($v = 1$) with He atom, in order to predict the quenching rate coefficient in a broad range of temperatures $5 < T < 2500$ K. Scattering calculations are done in two different ways: direct calculations of quenching cross sections and, alternatively, calculations of the excitation cross sections plus microscopic reversibility. In addition, a symmetrized average-velocity method of Billing is tried. Combination of these methods allows reproducing experiment in a broad range of temperatures. Excellent agreement with experiment is obtained at $400 < T < 2500$ K (within 10%), good agreement in the range $100 < T < 400$ K (within 25%), and semi-quantitative agreement at $40 < T < 100$ K(within a factor of 2). This study provides a stringent test of the mixed quantum/classical theory, because the vibrational quantum in CO molecule is rather large and the quencher is very light (He atom). For heavier quenchers and closer to dissociation limit of the molecule, the mixed quantum/classical theory is expected to work even better. © *2013 AIP Publishing LLC*. [http://dx.doi.org/10.1063/1.4818488]

I. INTRODUCTION

Collisional energy transfer in carbon monoxide plays a significant role in atmospheric chemistry,[1,2] astrophysics,[3–5] and condensed matter physics at ultra-cold temperatures.[6,7] It has been studied in the past both theoretically[8–19] and experimentally[3,18] in a broad range of temperatures. For example, rotational-vibrational transitions of CO is a valuable diagnostic probe of diverse astrophysical environments, such as interstellar and circumstellar media,[20–24] where the temperatures of interest are very high, up to $T \sim 2500$ K. Ro-vibrational transitions in the intermediate temperature range, $300\text{ K} < T < 1000$ K, are important to the post-combustion kinetics of CO.[23–25] Finally, these processes play critical role in developing the methods for cooling (and trapping) molecules to (at) sub-Kelvin temperatures, because efficiency of experimental techniques depends on the ratio between elastic and inelastic scattering cross sections. Thus, experimental studies of inelastic transitions in CO + He is an important benchmark, which has many potential applications including the high resolution molecular spectroscopy and controlled chemical reactions.[26,27] Also, the study of vibrational relaxation of CO by collisions with He atoms provides a convenient general model which could be used for analysis of relaxation processes involving other diatomic molecules and other low-mass collision partners.[13]

In the past, significant efforts have been devoted to testing and refining the potential energy surface (PES) for interaction between CO and He. Despite the fact that this system is relatively simple from the chemical point of view, a satisfactory agreement between calculated and experimental rate coefficients could not be achieved for a long period of time.[9–12,28] The improvement of detection techniques[29,30] and development of the PES[31–33] went through several refinement cycles. Finally, an acceptable agreement between theory and experiment has been reached in different parts of the desired broad range of temperatures. Two latest very similar PESs for this system have been reported[34,35] and used for calculations of inelastic scattering. The PES from Ref. 34 was used in this work in order to enable direct comparison of our results with those of Refs. 15 and 17.

Due to this past interest, the CO($v = 1$) + He seems to represent an ideal benchmark system for developing and testing new theoretical methods for description of ro-vibrational quenching. The exact inelastic quantum scattering approach (coupled-channel) is expected to be accurate, but appears to be computationally affordable for $T < 500$ K only.[9,15,16,18] At higher temperatures, the approximate quantum calculations (coupled states) are usually accurate in predicting the transition probabilities and cross sections, but inclusion of the highly excited rotational states is still very expensive.[16,17,36] In the contrast, the classical trajectory calculations, although highly affordable, are not able to provide good agreement with experimental data.[37] The main drawback of classical approach is leakage of zero-point energy, which becomes severe in the molecules with large vibrational quanta. Thus, it is desirable to develop an alternative method, which will work in the broad range of temperatures and for any molecule.

One reasonable way to tackle the inelastic ro-vibrational quenching is a mixed quantum/classical theory (MQCT) where the vibrational motion of the molecule is treated quantum mechanically while translational and rotational

a)Author to whom correspondence should be addressed. Electronic mail: dmitri.babikov@mu.edu

degrees of freedom are treated classically.[38] This approach eliminates the problem of zero-point energy leakage, and also allows capturing other quantum mechanical phenomena, such as scattering resonances (including calculations of their lifetimes[41,42]), quantization of vibrational states, their normal *vs.* local mode character, and finally, quantum symmetry.[43]

The MQCT method[39–42] is expected to work well when the rotational quantum is small compared to thermal energy. This condition may not be fulfilled entirely for the lightest rotors only, such as methane or water (both contain H atoms), but it is satisfied well for majority of molecules, including heavy diatomics such as CO, O_2, N_2, etc. The second requirement is a semi-classical regime of scattering. In this respect, the CO($v = 1$) + He system studied here is not an easy one. The helium atom is light and one expects to see deviations from classical scattering at lower temperatures.

So, the purpose of this work was to carry out calculations of ro-vibrational quenching using the MQCT method and compare results with experiment in a broad range of temperatures, in order to see whether the classical approximation breaks down or not and, if it does, at what temperature does this happen and how bad the MQCT results become, or they still remain acceptable? The findings from these calculations came out very encouraging.

Several sets of results in the range $5\,\mathrm{K} < T < 2500\,\mathrm{K}$ are presented, analyzed, and compared in this paper. Some of our results are from "direct" calculations of *quenching*, where the initial vibrational state of CO is $v = 1$, and cross sections for transitions to the final ground state $v = 0$ are computed directly and used to derive the quenching rates. Another set of data is from the "reverse" approach, where cross sections for *excitations* from $v = 0$ to $v = 1$ are computed first, and then converted into the quenching rates using the principle of microscopic reversibility.[19,44] One more set of data is from the average-velocity (symmetrized) approach of Billing,[45] where the principle of microscopic reversibility is built in by construction, and the results of direct and reverse calculations are very similar to each other.

The paper is organized as follows. In Sec. II, we outline major components of the MQCT for the simplest energy-transfer process – collision of a diatomic molecule with an atomic quencher. Numerical results for CO($v = 1$) + He are presented and discussed in Sec. III. The last Sec. IV is devoted to the symmetrized approach. Conclusions and possible applications of this theory are given in Sec. V.

II. THEORETICAL FRAMEWORK

Detailed derivations of equations for the mixed quantum/classical treatment of inelastic diatomic quencher + molecule scattering have been reviewed recently.[46] Here, we briefly recap only the major points of this theory.

A. Mixed quantum/classical dynamics

Vibrational motion of the molecule is treated quantum mechanically by introducing the vibrational wave function $\Psi(R, t)$ and propagating numerically the time-dependent Schrodinger equation,

$$i\frac{\partial}{\partial t}\Psi(R,t) = \hat{H}(t)\Psi(R,t), \tag{1}$$

on a grid of points using the wave packet technique.[47] The Hamiltonian operator

$$\hat{H}(t) = -\frac{\hbar^2}{2\mu}\frac{\partial^2}{\partial R^2} + V_{\mathrm{rot}}(R;t) + V_{\mathrm{pot}}(R;t) \tag{2}$$

is time-dependent (implicitly) because the centrifugal term

$$V_{\mathrm{rot}}(R;t) = \frac{p_\gamma^2}{2\mu R^2} + \frac{p_\alpha^2}{2\mu R^2 \sin^2\gamma} \tag{3}$$

and the potential energy surface $V_{\mathrm{pot}}(R;t) = V_{\mathrm{pot}}(R, \alpha, \gamma, \mathbf{q})$ both depend on the classical variables: $\alpha(t)$, $\gamma(t)$, and $\mathbf{q}(t)$. Azimuthal angle α and polar angle γ describe orientation of the molecule in space. Its rotational motion is treated classically by introducing their conjugate momenta $p_\alpha(t)$ and $p_\gamma(t)$, and propagating the Hamiltonian equations

$$\dot{\alpha} = \frac{p_\alpha}{\tilde{I}\sin^2\gamma}, \tag{4a}$$

$$\dot{\gamma} = \frac{p_\gamma}{\tilde{I}}, \tag{4b}$$

$$\dot{p}_\alpha = -\frac{\partial\tilde{V}}{\partial\alpha}, \tag{4c}$$

$$\dot{p}_\gamma = -\frac{\partial\tilde{V}}{\partial\gamma} + \frac{p_\alpha^2\cos\gamma}{2\tilde{I}\sin^3\gamma}. \tag{4d}$$

The instantaneous mean moment of inertia $\tilde{I}(t)$ of such "fluid" rotor is determined by vibrational wave function[39,46]

$$\tilde{I}(t) = \langle\Psi(R,t)|\frac{1}{\mu R^2}|\Psi(R,t)\rangle^{-1}. \tag{5}$$

The mean-field potential

$$\tilde{V}(\alpha,\gamma,\mathbf{q},t) = \langle\Psi(R,t)|V_{\mathrm{pot}}(R,\alpha,\gamma,\mathbf{q})|\Psi(R,t)\rangle, \tag{6}$$

drives the classical trajectory of motion for rotation and the process of quencher + molecule scattering, described by Cartesian coordinates $\mathbf{q}(t)$ and their conjugate momenta $\mathbf{p}(t)$

$$\dot{\mathbf{q}} = \mathbf{p}/m, \tag{7a}$$

$$\dot{\mathbf{p}} = -\nabla\tilde{V}. \tag{7b}$$

In this way, the vibrational motion, treated with quantum mechanics, affects the classical degrees of freedom (rotation and scattering) through the mean values of $\tilde{I}$ and $\tilde{V}$ in Eqs. (4) and (7). In turn, the classical trajectory for rotation and scattering affects evolution of quantum vibrational wave function, through time-dependence of V_{rot} and V_{pot} in the Hamiltonian operator of Eq. (2). Energy is exchanged between vibrational, rotational, and scattering degrees of freedom, while the total energy is conserved. Spectral analysis of the final vibrational wave packet gives information about probabilities of state-to-state transitions $P_{vv'}^{jj'}(E)$, which is easy to convert into cross sections $\sigma_{vv'}^{jj'}(E)$, as shown below.

B. Quenching rate coefficient from direct calculations

In this section, we will discuss ro-vibrational transitions and will label final states by primed indexes. For example, cross section for a transition from the initial ro-vibrational state (v, j) into the final state (v', j') at collision energy E is denoted by $\sigma_{vv'}^{jj'}(E)$. Quantum mechanical expression for the rate coefficient of vibrational quenching from $v = 1$ into $v' = 0$ is[15–17,19]

$$\kappa_{10}^{\rm dir}(T) = \sqrt{\frac{8kT}{\mu\pi}}\frac{1}{(kT)^2} \times \frac{\sum_{j'}\sum_{j}(2j+1)\exp\left(-\frac{\varepsilon_1^j}{kT}\right)\int_0^\infty \sigma_{10}^{jj'}(E)E\exp\left(-\frac{E}{kT}\right)dE}{\sum_j(2j+1)\exp\left(-\frac{\varepsilon_1^j}{kT}\right)}. \quad (8)$$

Note that in this expression cross sections for the vibrational transition of interest (from $v = 1$ to $v' = 0$) are summed over the final rotational states (j') and are averaged over the initial rotational states (j), assuming thermal distribution and taking into account the rotational degeneracy. Ro-vibrational energies of the initial states are denoted by ε_1^j. Subscript "dir" means that these are "direct" calculations of quenching, as opposed to "reverse" calculations discussed in Sec. II C.

Now recall that in our approach the rotational motion is treated classically. Distributions of the initial and final rotational states are continuous and smooth (not quantized). In this situation, Eq. (8) should be rewritten in the following way:

$$\kappa_{10}^{\rm dir}(T) = \sqrt{\frac{8kT}{\mu\pi}}\frac{1}{(kT)^2}\int_0^\infty \tilde{\sigma}_{10}(E)E\exp\left(-\frac{E}{kT}\right)dE, \quad (9)$$

where we introduced

$$\tilde{\sigma}_{10}(E) = \frac{\sum_{j'}\sum_{j}(2j+1)\exp\left(-\frac{\varepsilon_1^j}{kT}\right)\sigma_{10}^{jj'}(E)}{\sum_j(2j+1)\exp\left(-\frac{\varepsilon_1^j}{kT}\right)}. \quad (10)$$

This emphasizes that only the vibrational motion is quantized, while the rotational motion is treated classically. Strictly speaking, our mixed quantum/classical calculations cannot produce well-defined values of the individual $\sigma_{10}^{jj'}$. They can only give the average value of $\tilde{\sigma}_{10}$.

From practical perspective, this also means that sampling of the initial rotational states can be optimized (at a given T) for calculations of $\tilde{\sigma}_{10}(E)$ as a whole. There is no need to converge the value of each individual $\sigma_{10}^{jj'}(E)$; only the accuracy of average $\tilde{\sigma}_{10}(E)$ matters. In this respect, some values of j are more important than others and it is convenient to introduce *weights* of the initial ro-vibrational states as

$$w_v^j(T) = \frac{(2j+1)\exp\left(-\frac{\varepsilon_v^j}{kT}\right)}{\sum_j(2j+1)\exp\left(-\frac{\varepsilon_v^j}{kT}\right)}. \quad (11)$$

Using this definition, we can convert Eq. (10) into

$$\tilde{\sigma}_{10}(E) = \sum_j w_1^j \sum_{j'}\sigma_{10}^{jj'}(E). \quad (12)$$

This transparent expression emphasizes summation over the final j' and averaging (weighted sum) over the initial j.

C. Quenching rate coefficient from microscopic reversibility

Microscopic reversibility plays fundamental role in the reaction dynamics.[44] In practice, it is sometimes advantageous to carry out calculations in the "reverse" direction (e.g., excitation instead of quenching) and then convert these raw data into the final data for "direct" process, using the principle of microscopic reversibility.[21,44,49] This approach works well for the full-quantum dynamics.[48] In the mixed quantum/classical dynamics, the microscopic reversibility is not automatically built in,[45] and we felt it is important to do calculations in the reverse direction as well, namely, for collisional excitation from $v' = 0$ into $v = 1$.

Calculations carried out for vibrational excitation at collision energy E' give us cross sections $\sigma_{01}^{j'j}(E')$. In notations of this section, we switch the order of indexes, because the process is reversed, but we still keep association of unprimed and primed indexes with excited and ground vibrational states, respectively. The principle of microscopic reversibility states that[49]

$$(2j+1)\sigma_{10}^{jj'}(E)E = (2j'+1)\sigma_{01}^{j'j}(E')E'. \quad (13)$$

This assumes that the total energy (collisional + internal) of the direct processes is equal to that of the reverse process

$$E + \varepsilon_1^j = E' + \varepsilon_0^{j'}. \quad (14)$$

Rotational energy is included into the ro-vibrational eigenvalues ε_1^j and $\varepsilon_0^{j'}$, but it gives minor contribution compared to the quantum of vibration: $\Delta\varepsilon = \varepsilon_1^0 - \varepsilon_0^0 \approx 2143\,\text{cm}^{-1}$ (using the PES of CO from Ref. 15). Thus, for CO, calculations of direct and reverse processes should be carried out at very different collision energies. For example, if for the direct process $E = kT \approx 200\,\text{cm}^{-1}$ at room temperature, then for the reverse process $E' \approx E + \Delta\varepsilon = 2343\ \text{cm}^{-1} \approx 12\,kT$.

Substitution of Eqs. (13) and (14) into Eq. (8) allows obtaining the following formula (see the Appendix):

$$\kappa_{10}^{\rm rev}(T) \approx \sqrt{\frac{8kT}{\mu\pi}}\frac{1}{(kT)^2} \times \int_0^\infty \tilde{\sigma}_{01}(E+\Delta\varepsilon)(E+\Delta\varepsilon)\exp\left(-\frac{E}{kT}\right)dE, \quad (15)$$

where rate coefficient of the direct process κ_{10} is expressed through average cross section for the reverse process $\tilde{\sigma}_{01}(E + \Delta\varepsilon)$. We see that, indeed, the scattering calculations of the reverse process should be carried out at energy raised by $\Delta\varepsilon$, compared to calculations of the direct process.

Note that Eq. (15) is approximate. In order to make this formula look similar to Eq. (9), we used two approximations described in the Appendix, but they hold well for the CO + He quenching. Furthermore, those approximations are related to how the rotational energy is treated. In the absence of rotation, Eq. (15) is exact. The general expression is also discussed in the Appendix.

D. Numerical approach

The initial conditions for CO + He collisions were generated in the following way. At $t = 0$, the center of mass of CO is at the origin of the laboratory reference frame, while He is at a distance of ~35 bohrs. The incident direction of He atom is sampled randomly and uniformly as explained in Ref. 46. The impact parameter b is sampled randomly and uniformly (independently from sampling the incident direction) in the range $0 \le b \le b_{\max}$, where $b_{\max} = 8$ bohrs. Initial momenta $p(t = 0) = \sqrt{2\mu E}$ of the incident He atoms are determined by the center-of-mass collision energy E, constant for a batch of trajectories.

The initial rotational states of CO are chosen randomly, but taking into account their weights in Eq. (11). For example, for the direct calculations (quenching) at a given temperature T, first, the weights $w_1^j(T)$ are computed and truncated at some large value of j, giving n_j numbers. Then, the range [0, 1] is split onto n_j intervals with lengths proportional to $w_1^j(T)$. Finally, a random number is generated in the range [0, 1] and the initial rotational state j is chosen based on which of n_j sectors this number falls in.

When the initial rotation state j is chosen, the vibrational eigenstate $v = 1$ is computed for the Hamiltonian (2) with $V_{\rm rot}(R;t) = j^2/(2\mu R^2)$ and is used to set up the initial wave packet $\Psi(R, t = 0)$. The non-uniform grid of 64 points is optimized as explained in Ref. 39. The initial values of classical variables for rotation are $\alpha = 0$, $\gamma = \pi/2$, $p_\gamma = 0$, and $p_\alpha = j$. Classical equations of motion are propagated using 4th-order Runge-Kutta method with adaptive step-size control.[50] Vibrational wave packet is propagated using Lanczos method.[51] Kinetic energy operator is applied using FFT.[50]

At the final moment of time, the spectrum of vibrational eigenstates of the final rotational state $j' = \sqrt{p_\gamma^2 + p_\alpha^2/\sin^2\gamma}$ is computed, and the vibrational wave packet $\Psi(R, t)$ is projected onto $v' = 0$ to obtain the corresponding transition probability $P_{10}^{jj'}(E)$. If needed, these could be converted into individual cross sections $\sigma_{10}^{jj'}(E)$ by binning the values of final j' (the values of initial j are already integer by set up). Instead, we focused on computing the rotationally averaged cross sections for vibrational quenching $\tilde{\sigma}_{10}(E)$ using

$$\tilde{\sigma}_{10}(E) = 2\pi b_{\max} \sum_{n=1}^{N} b P_{10}^{jj'}(E)/N. \qquad (16)$$

In this expression, the sum over N trajectories in a batch replaces two sums in Eq. (12) – the simple sum over final j' and the weighted sum over initial j.

For calculations in the reverse direction (excitation) the procedure is similar, but the weights $w_0^{j'}(T)$ are used and the initial wave function is that of $v' = 0$ eigenstate. The incident momentum $p'(t = 0) = \sqrt{2\mu E'}$ is determined by $E' = E + \Delta\varepsilon$, and the final projection is onto $v = 1$ eigenstate. The result of such calculation is $\tilde{\sigma}_{01}(E + \Delta\varepsilon)$.

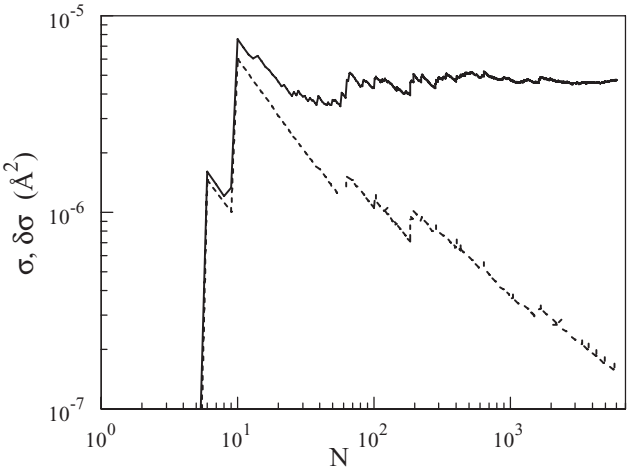

FIG. 1. Convergence of average excitation cross section $\tilde{\sigma}_{01}$ (solid line) and its statistical error $\delta\tilde{\sigma}_{01}$ (dotted line) as a function of the number of trajectories N in a sample.

Figure 1 gives example of convergence study for $\tilde{\sigma}_{01}(E)$ at $E = 800\,\text{cm}^{-1}$ and $T = 200$ K. The value of statistical error $\delta\tilde{\sigma}$ is also shown. We see that after $N \sim 6000$ trajectories the error drops to the level of ~2%, which we consider a converged result. It is worth noting, and is rather surprising, that after only as few as 20 trajectories one gets a reasonable estimate of averaged cross section $\tilde{\sigma}$. Of course, after 20 trajectories the statistical error is still high, $\delta\tilde{\sigma} = 60\%$. Anyway, this is a very useful property: it appears that one can generate a good estimate of rotationally averaged $\tilde{\sigma}$ at very little computational cost. This must be due to efficiency of the multi-dimensional Monte Carlo integration in Eq. (16), which utilizes the importance sampling according to the weights w_v^j given by Eq. (11). In Table I, we listed how many values of j were included in Eq. (10) and how many trajectories were propagated in Eq. (16), in order to obtain converged results at different temperatures.

TABLE I. Requirements and convergence in terms of the rotational excitation and the number of trajectories in the MQCT calculations at different temperatures.

T (K)	j_{max}	N	$\delta\sigma/\sigma \times 100\%$
5[a]	2	120	31
20[a]	5	120	33
50[a]	9	240	25
100	18	3800	2
500	35	4700	2
1000	52	5900	2
1500	64	7800	2
2000	70	8600	2
2300	75	9500	2

[a]At these temperatures, the results are not entirely converged, obtained for an estimate only.

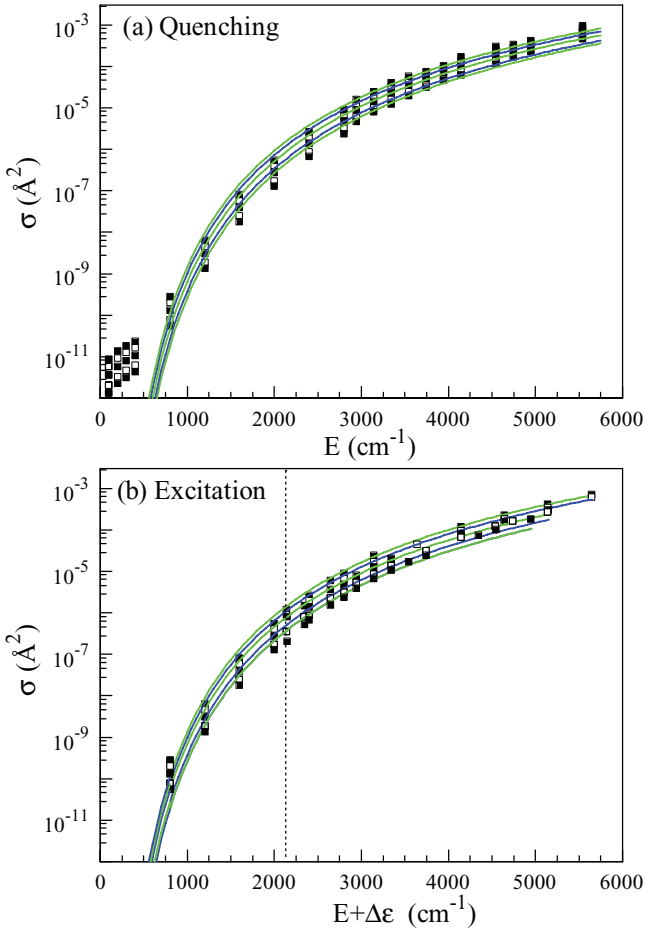

FIG. 2. Computed cross sections (symbols) and their analytic fits (lines) for: (a) quenching $\tilde{\sigma}_{10}(E)$; and (b) excitation $\tilde{\sigma}_{01}(E+\Delta\varepsilon)$. Each frame shows data obtained at five values of temperature: from $T = 100$ K to $T = 900$ K with 200 K steps. Vertical dotted line in frame (b) corresponds to $E = 0$, or $E' = \Delta\varepsilon$.

III. RESULTS AND DISCUSSION

Figure 2(a) shows examples of computed cross sections for quenching, $\tilde{\sigma}_{10}(E)$, in a broad range of relevant energies for five chosen values of temperature: from $T = 100$ K to $T = 900$ K with 200 K steps. Figure 2(b) shows the same for excitation, $\tilde{\sigma}_{01}(E+\Delta\varepsilon)$. Note that Figs. 2(a) and 2(b) have different horizontal axes: E and $E+\Delta\varepsilon$, respectively. The overall trends of $\tilde{\sigma}_{10}(E)$ and $\tilde{\sigma}_{01}(E+\Delta\varepsilon)$ are similar (except at low energies, see below). Their monotonic behavior is easy to fit by the well-known analytic expression for energy dependence of state-to-state transition cross section[52]

$$\sigma(E) = aE\exp(-b/\sqrt{E}). \tag{17}$$

The fitting coefficients a and b carry physical meaning: a corresponds to the average magnitude (well depth) while b corresponds to the average distance (well size) of the molecule + quencher interaction potential. We found that this dependence describes well both excitation and quenching processes – $\tilde{\sigma}_{10}(E)$ and $\tilde{\sigma}_{01}(E+\Delta\varepsilon)$, with E in Eq. (17) replaced by $E+\Delta\varepsilon$ for the latter case, and slightly different fitting coefficients. The coefficients are collected in Table II. The dependencies of $a(T)$ and $b(T)$ on temperature are smooth and monotonic.

TABLE II. Temperature dependence of fitting coefficients in the analytic expression for excitation and quenching cross sections.

	$a \times 10^3$ (Å^2/cm^{-1})		$b \times 10^{-2}$ (cm$^{-1/2}$)	
T (K)	Excitation	Quenching	Excitation	Quenching
100	1.66	1.61	7.51	7.47
200	1.65	1.60	7.43	7.39
300	1.65	1.60	7.35	7.32
400	1.64	1.60	7.28	7.24
500	1.62	1.59	7.22	7.15
600	1.62	1.58	7.12	7.06
700	1.61	1.55	7.05	6.98
800	1.58	1.51	7.00	6.91
900	1.52	1.47	6.93	6.83

The quenching cross section $\tilde{\sigma}_{10}(E)$ tends to vanish as $E \to 0$. Four points computed in the range $E < 500$ cm^{-1} exhibit cross sections on order of $\tilde{\sigma}_{10} \approx 10^{-11}$ Å^2, and this is probably an overestimation. These numbers may not be particularly accurate because they are so small. The fit using Eq. (17), with these points excluded, suggests even smaller values for quenching cross section at $E < 500$ cm^{-1}.

In contrast, the excitation cross section $\tilde{\sigma}_{01}(E+\Delta\varepsilon)$ is finite (non-zero) at $E = 0$ and exhibits values on order of $\tilde{\sigma}_{01} \approx 10^{-6}$ Å^2. Note that the values of excitation cross sections $\tilde{\sigma}_{01}(E+\Delta\varepsilon)$ are finite even at $E \le 0$ (in Fig. 2(b), this part of energy range is to the left of the vertical dashed line $E' = \Delta\varepsilon$). This is so because, as explained in Sec. II D, the reverse calculations are done at collision energy $E' = E + \Delta\varepsilon$. At $E = 0$, we still have some residual collision energy $E' = \Delta\varepsilon \approx 2143$ cm^{-1}, just sufficient to reach the channel threshold. Below this energy the quantum mechanical cross section for excitation would be zero, but the MQCT approach yields a (small but) non-zero cross section at $E < 0$. This is an artifact, apparently, due to the mean-field treatment of collision. According to Eq. (15), the energy range $E < 0$ is not included in the integral of the rate coefficient $\kappa_{10}^{\rm rev}$.

To further clarify this point, we plotted in Figs. 3(a) and 3(b) the values of integrand in Eq. (9) for direct calculations $f^{\rm dir}(E) = \tilde{\sigma}_{10}(E)E\exp\{-E/kT\}$ and in Eq. (15) for reverse calculations $f^{\rm rev}(E') = \tilde{\sigma}_{01}(E')E'\exp\{-(E'-\Delta\varepsilon)/kT\}$, respectively. One sees that in Fig. 3(a) the integrand vanishes at $E = 0$ as it should, while in Fig. 3(b) the integrand is finite at $E = 0$. At higher temperatures, this does not affect the value of κ_{10} significantly, since the integrand shows maximum at $E > 0$, and its behavior near $E = 0$ is less important. However, at $T \le 400$ K the maximum of the integrand is at $E \le 0$ (to the left of the vertical dashed line $E' = \Delta\varepsilon$) so that the energy region near $E = 0$ plays the dominant role. Thus, the artificially large values of $\tilde{\sigma}_{01}(E+\Delta\varepsilon)$ at low energies E lead to artificially large values of integrand in Eq. (15) which, at the end, may result in overestimated values of $\kappa_{10}(T)$ at low temperatures.

The results for $\kappa_{10}(T)$ from direct and from reverse calculations, and the available experimental data,[4,20,53] are shown all together in Fig. 4 (solid lines for calculations, symbols for experiments). The $\kappa_{10}(T)$ dependence from direct calculations shows correct trend in the entire range of temperatures, but

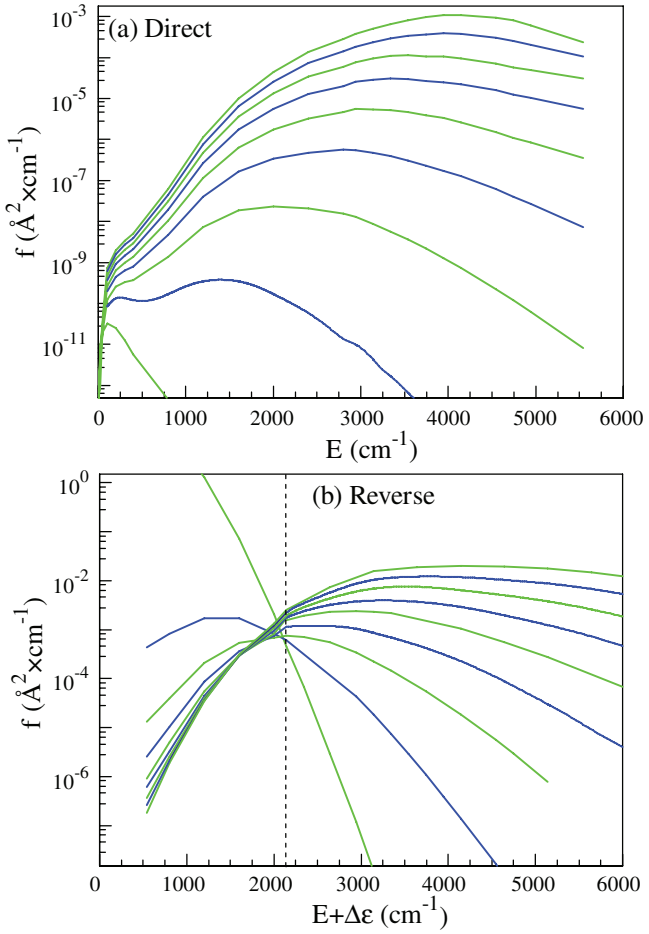

FIG. 3. Energy dependence of the integrand in the expression for quenching rate coefficient: (a) $f^{\rm dir}(E)$ in Eq. (9) for direct calculations; and (b) $f^{\rm rev}(E+\Delta\varepsilon)$ in Eq. (15) for reverse calculations. Each frame shows data obtained at nine values of temperature: from $T = 100$ K to $T = 900$ K with 100 K steps. Vertical dotted line in frame (b) corresponds to $E = 0$, or $E' = \Delta\varepsilon$.

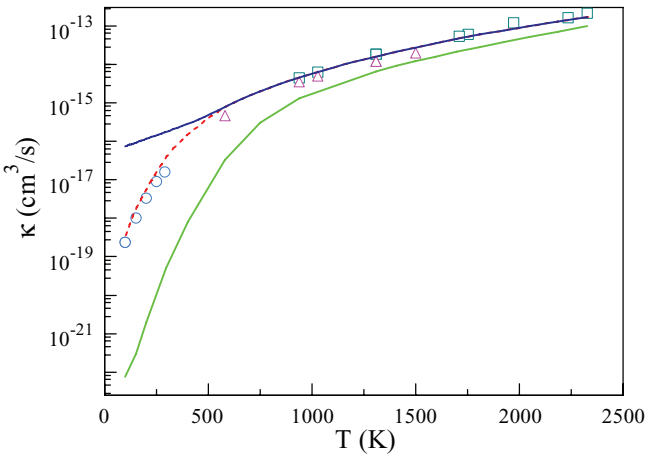

FIG. 4. Rate coefficients for quenching of CO($v = 1$) by He impact from direct calculations (solid green line) and from reverse calculations (solid blue line), in comparison to experimental results (symbols) taken from Refs. 4, 18, and 51. Dashed red line shows results of empirical correction to the reverse approach at low collision energies. See text for details.

the absolute values are underestimated compared to experiment, particularly at low temperatures (three orders of magnitude difference at $T = 100$ K). Interestingly, the $\kappa_{10}(T)$ dependence from reverse calculations follows experiment very closely at all temperatures higher than $T \approx 400$ K. However, at $T \le 400$ K the reverse calculations deviate from the experiment up, giving overestimated values of $\kappa_{10}(T)$, which could be expected from the discussion above.

Given the success of reverse approach at $T > 400$ K, it would be desirable to find a practical fix for the problem at low temperatures. An *ad hoc* solution is simply to force $\tilde{\sigma}_{01}(E+\Delta\varepsilon)$ to go to zero at $E = 0$, analytically. We tried this, and multiplied the computed cross section $\tilde{\sigma}_{01}(E+\Delta\varepsilon)$ by a smooth masking function (related to arctangent) that starts from zero at $E = 0$ and goes to one at $E \approx 700\,{\rm cm}^{-1}$. Same function was used for all temperatures. The result is in excellent agreement with experiment in the entire range of temperatures (see Fig. 4, dashed line). Although this approach is entirely empirical, its simplicity and success makes it quite useful.

It is worth noting that at high temperatures we see a much better agreement between direct and reverse calculations. For example, at $T = 2300$ K two values of κ_{10} are less than one order of magnitude different (75% different, to be more precise) and the trend is such that at even higher temperatures the difference is expected to decrease even further. Recall that direct and reverse calculations are done with two different collision energies, E and $E+\Delta\varepsilon$, respectively. When E is small the effect of extra-energy (equal to the vibrational quantum $\Delta\varepsilon$) is very significant, but when energy E is high by itself the effect of $\Delta\varepsilon$ is much less important. So, one can deduce that the difference between direct and reverse calculations is manifestation of quantization of vibrational states in the MQCT method. In the case of CO, the vibrational quantum is particularly large, $\Delta\varepsilon = 2143\,{\rm cm}^{-1}$, and it is not surprising that high temperature is needed in order to see the direct and reverse results merging to the same value of κ_{10}. Indeed, the quenching of fundamental transition in CO($v = 1$) is one of the worst case scenarios. Near the dissociation limit, where the density of states is much higher, the mixed quantum classical method would work much better.

Moreover, the problem of non-vanishing $\tilde{\sigma}_{01}(E+\Delta\varepsilon)$ at $E = 0$ (discussed above) is also related to the large value of quantum $\Delta\varepsilon$ in CO. If $\Delta\varepsilon$ would be smaller, the value of $\kappa_{10}(T)$ from reverse calculations would agree with experiment even at lower temperatures. In order to test this hypothesis, we carried out a set of additional calculations for one chosen value of $T = 300$ K, but for several different CO molecules. Impossible in experiment, but straightforward in theory is to flatten the PES of CO, producing new molecule with smaller vibrational quantum! In such computational experiments, we studied the values of vibrational quantum down to $\Delta\varepsilon = 100\,{\rm cm}^{-1}$. Figure 5(a) gives the values of $\kappa_{10}^{\rm rev}$ and $\kappa_{10}^{\rm dir}$ vs. $\Delta\varepsilon$, while Figure 5(b) gives the ratio $R = (\kappa_{10}^{\rm rev} - \kappa_{10}^{\rm dir})/(\kappa_{10}^{\rm rev} + \kappa_{10}^{\rm dir})$. The last points in Figs. 5(a) and 5(b) corresponds to true CO, where at $T = 300$ K the value of κ_{10} obtained from the reverse calculations is several orders of magnitude larger than that obtained from the direct calculations. In this case, the ratio R is very close to one. As we reduced $\Delta\varepsilon$, we first saw a plateau for the ratio R, expanding down to $\Delta\varepsilon \sim 1000\,{\rm cm}^{-1}$, but then, in the range of

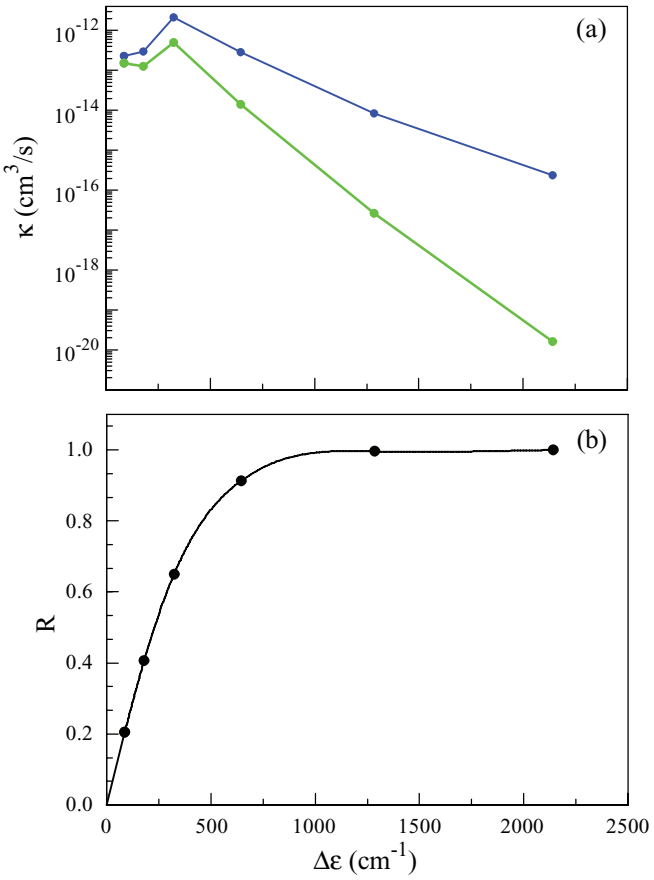

FIG. 5. The dependence of: (a) $\kappa_{10}^{\rm rev}$ and $\kappa_{10}^{\rm dir}$, and (b) the ratio $R = (\kappa_{10}^{\rm rev} - \kappa_{10}^{\rm dir})/(\kappa_{10}^{\rm rev} + \kappa_{10}^{\rm dir})$, on the value of vibrational quantum $\Delta\varepsilon$ in a series of computational experiments with theoretically modified CO potential.

$\Delta\varepsilon < 400\,{\rm cm}^{-1}$, we observed a fast (close to linear) decrease of the ratio R down to zero (see Fig. 5(b)). At $\Delta\varepsilon = 100\,{\rm cm}^{-1}$, the values of κ_{10} from direct and reverse calculations were only 20% different.

We believe this numerical experiment proves that direct and reverse calculations are expected to be equivalent (and, in fact, both accurate) in the semi-classical regime, when the vibrational quantum $\Delta\varepsilon$ is on the order of thermal energy, or smaller. However, our results for CO with large vibrational quantum show that at low temperatures they produce different results, which means that microscopic reversibility is not built automatically in the MQCT method.

IV. THE AVERAGE VELOCITY (SYMMETRIZED) APPROACH

During the process of finalizing this paper, we run onto a book of Billing,[45] which we did not know about. It appears that Billing[45] found an ingenious solution that allows merging the results of direct and reverse calculations, even in the case of low temperature and large vibrational quantum $\Delta\varepsilon$. We are not going to repeat his arguments here, but will present our own viewpoint on his method.

We believe that the problem of unsatisfied reversibility is due to the Ehrenfest (mean-field) treatment of the scattering process in the MQCT method. Indeed, in the full-quantum approach the incoming wave in the entrance channel and the outgoing wave in the exit channel of the process correspond to two different energies (very different in the case of large vibrational quantum $\Delta\varepsilon$). The approximate method of trajectory surface hopping[54] takes this information into account, by adjusting momentum in the exit channel to reflect the change of internal energy (by $\Delta\varepsilon$). But the Ehrenfest approach is, in a sense, an antithesis of the trajectory surface hopping. If the transition probability is very small (which is the case here at low T), the trajectory in the inelastic exit channel is almost equivalent to the elastic trajectory, because the mean field potentials, given by Eq. (6), are very similar and momenta are very close to $p = \sqrt{2\mu E}$. In order to fix the Ehrenfest approach, we must use, somehow, the information from reverse trajectories that have momentum $p' = \sqrt{2\mu E'}$, which corresponds to energy of the exit channel $E' = E + \Delta\varepsilon$. Our results for CO presented above show that experiment is between the direct and reverse results, which is encouraging.

A. Transition cross-section

One technical thing we have to do first is to replace the classical-like expression for cross section, Eq. (16), with a quantum-like formula

$$\sigma_{10}^{jj'} = \frac{\pi}{k^2}\sum_{J=0}^{J_{\max}} \frac{1}{N_J}\frac{(2J+1)}{(2j+1)} \sum_{l=|J-j|}^{l=J+j} P_{10}^{jj'}. \qquad (18)$$

Here, J is total angular momentum of the molecule + quencher system, l is orbital momentum of the quencher. As in Eq. (16), the probability is summed over the final rotational states but Eq. (18) is for one given value of j; it should be thermally averaged over the initial j, similar to Eq. (10). This expression originates from the standard full-quantum expression.[55]

Practical implementation of this formula uses sampling procedure different from the one described in Sec. II D. Here, for each given j one should sample J randomly and uniformly between 0 and $J_{\max}$ (determined by $b_{\max}$) and then sample l randomly and uniformly between $|J - j|$ and $J + j$. However, we checked and found that both sampling methods produce practically equivalent distributions. We also checked and found that expressions of Eqs. (16) and (18) give very similar results for cross sections. Indeed, one can show that in the limit of small j and high collision energy, when $J \approx l$ (here we take $j = 0$ for simplicity) and $l \approx bk$, which follows from $l(l+1) = (bk)^2$, expression of Eq. (18) gives

$$\sigma \approx \frac{\pi}{k^2}\sum_l \frac{(2l+1)}{N_l} P = \frac{\pi}{k^2}\frac{l_{\max}}{N}\sum_l (2l+1)P$$
$$\approx \frac{\pi}{k^2}\frac{l_{\max}}{N}\sum 2bkP = \frac{2\pi b_{\max}}{N}\sum bP, \qquad (19)$$

equivalent to Eq. (16). Our numerical results showed that Eq. (16) slightly underestimates cross section compared to Eq. (18), but (even in the worst case of low collision energy, $E = \Delta\varepsilon/4 \sim 536\,{\rm cm}^{-1}$) by no more than 20%.

B. Microscopic reversibility

An important property of Eq. (18), in the context of reversibility, is the explicit dependence of cross section on collision energy ($k^2 = 2\mu E/\hbar^2$ in the case of direct and $k'^2 = 2\mu E'/\hbar^2$ in the case of reverse calculations) and on rotational degeneracy ($2j+1$ and $2j'+1$, respectively). Substitution of Eq. (18) into the principle of microscopic reversibility, Eq. (13), leads to numerous cancellations and gives

$$P_{10}^{jj'}(E) = P_{01}^{j'j}(E'). \tag{20}$$

This expression tells us that microscopic reversibility is satisfied only if the transition probabilities for direct and reverse processes are equal. (Note that this is third version of the principle, now in terms of individual trajectories, in addition to that in terms of cross sections in Eq. (13), and rate coefficients in Eq. (A8).)

Now recall that probability of vibrationally inelastic (and in general any non-adiabatic) transition depends on collision velocity. We cannot possibly satisfy Eq. (20) at low energy E if $p = \sqrt{2\mu E}$ but $p' = \sqrt{2\mu(E+\Delta\varepsilon)}$ (i.e., much larger). One straightforward solution to the problem would be to launch direct and reverse trajectories with *equal* velocities. The average between direct and reverse velocities seems to be a reasonable chose, which leads to: $(\sqrt{E} + \sqrt{E+\Delta\varepsilon})/2 = \sqrt{U}$, where we introduced the *actual* collision energy U that permits to satisfy microscopic reversibility. This equation can be easily solved for E (taking square of left and right parts, twice) which gives

$$E = U - \frac{\Delta\varepsilon}{2} + \frac{\Delta\varepsilon^2}{16U}. \tag{21}$$

In a similar way, starting with $(\sqrt{E'-\Delta\varepsilon} + \sqrt{E'})/2 = \sqrt{U}$, one obtains

$$E' = U + \frac{\Delta\varepsilon}{2} + \frac{\Delta\varepsilon^2}{16U}. \tag{22}$$

Note that these expressions satisfy $E' = E + \Delta\varepsilon$ and $E < U < E'$.

Thus, in the symmetrized approach we will satisfy microscopic reversibility through $P_{10}^{jj'}(U) = P_{01}^{j'j}(U)$, but then we will express E and E' through U according to Eqs. (21) and (22), and will integrate the resultant probabilities in Eq. (9) for direct and in Eq. (A10) for reversed processes, using cross section in the form of Eq. (18). An important thing to note is that k^2 in the denominator of Eq. (18) should correspond to the integration variable, namely, $k^2 = 2\mu E/\hbar^2$ in the case of direct and $k'^2 = 2\mu E'/\hbar^2$ in the case of reverse calculations.

Furthermore, one can express U through E

$$U = \frac{E + \sqrt{E(E+\Delta\varepsilon)}}{2} + \frac{\Delta\varepsilon}{4}, \tag{23}$$

or U through E'

$$U = \frac{E' + \sqrt{E'(E'-\Delta\varepsilon)}}{2} + \frac{\Delta\varepsilon}{4}. \tag{24}$$

These expressions show that at the lower integration limit in Eq. (9), when $E = 0$, we have $U = \Delta\varepsilon/4$. Similarly, at the lower integration limit in Eq. (A10), when $E' = \Delta\varepsilon$, we have $U = \Delta\varepsilon/4$. So, the actual collision energy U of our trajectories is never less than one quarter of the vibrational quantum. In the case of CO quenching, this is about $E = 536\ \mathrm{cm}^{-1}$.

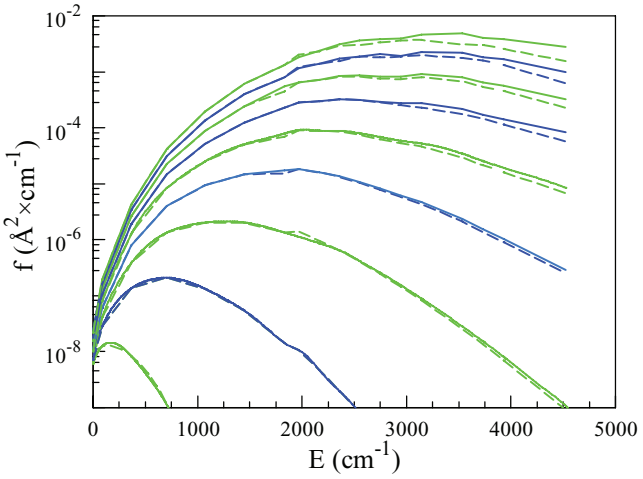

FIG. 6. Energy dependence of the integrands $f^{\mathrm{dir}}(E)$ of Eq. (25) and $f^{\mathrm{rev}}(E)$ of Eq. (27) for the symmetrized average-velocity approach. The data obtained at nine values of temperature are presented: from $T = 100$ K to $T = 900$ K with 100 K steps. Note that results from both direct (solid line) and reverse (dashed line) calculations are shown in one frame.

C. Numerical results

It has to be stressed that in order to implement the symmetrized average-velocity approach, we did not have to redo the scattering calculations. All we had to do was to reintegrate the cross sections we already had from the direct and reverse calculations discussed in Sec. III, but treating E and E' in their old meaning as U in its new meaning. Namely, for the direct process we integrated over E from 0 to $+\infty$, according to Eq. (9), the following integrand:

$$f^{\mathrm{dir}}(E) = \tilde{\sigma}_{10}(U)E\exp\{-E/kT\}, \tag{25}$$

where the $U = U(E)$ dependence is that of Eq. (23) and where for the reverse process we integrated over E' from $\Delta\varepsilon$ to $+\infty$, according to Eq. (A10), the following integrand:

$$f^{\mathrm{rev}}(E') = \tilde{\sigma}_{01}(U)E'\exp\{-(E'-\Delta\varepsilon)/kT\}, \tag{26}$$

where the $U = U(E')$ dependence is that of Eq. (24). Alternatively, for the reverse process one can re-express $f^{\mathrm{rev}}(E')$ through E

$$f^{\mathrm{rev}}(E) = \tilde{\sigma}_{01}(U)E\exp\{-E/kT\}, \tag{27}$$

and integrate it from 0 to $+\infty$, according to Eq. (A11).In Fig. 6, we plotted $f^{\mathrm{dir}}(E)$ and $f^{\mathrm{rev}}(E)$ together, using solid and dashed lines, respectively, for nine chosen values of temperature from $T = 100$ K to $T = 900$ K with 100 K steps. This picture demonstrates very clearly that $f^{\mathrm{dir}}(E) \cong f^{\mathrm{rev}}(E)$, particularly at low energies. It is almost unbelievable that Fig. 6 contains all exactly the same data as Figs. 3(a) and 3(b), only their arrangement is different (now in terms of $U = U(E)$).

The results for $\kappa_{10}(T)$ from the symmetrized calculations, both direct and reverse (lines), are shown in Fig. 7 and compared to available experimental data (empty symbols).

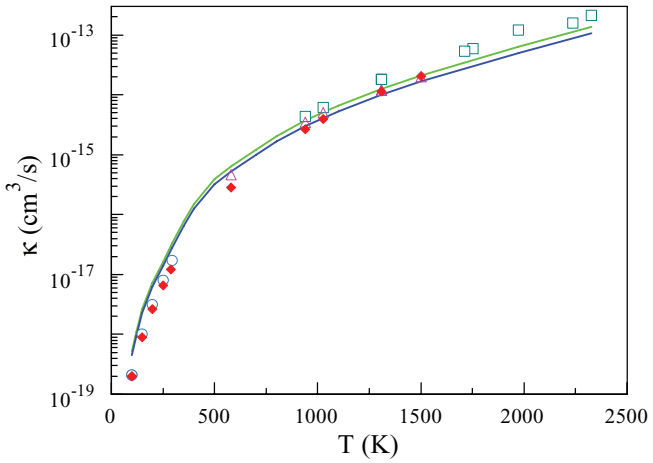

FIG. 7. Rate coefficients for quenching of CO($v = 1$) by He impact obtained according to the symmetrized average-velocity approach from direct (green line) and reverse (blue line), calculations. Experimental results from Refs. 4, 18, and 53 are shown by empty symbols. Full quantum results from Ref. 35 are shown by filled red diamonds.

The results from direct and reverse calculations are very close to each other, particularly at low temperatures, when transition probabilities are small and the perturbative picture discussed in Sec. IV B is applicable. The experimental dependence of $\kappa_{10}(T)$ is reproduced really well by these calculations, through the six orders of magnitude range of values and in a broad range of temperatures, without any empirical adjustments. The MQCT results also compare well with full quantum results of Peterson and McBane from Ref. 35 shown in Fig. 7 by filled red diamonds (obtained using a different PES).

Finally, we looked at the very low temperature range, where the full quantum calculations of Balakrishnan[15] showed the switch of the monotonic $\kappa_{10}(T)$ behavior near the $T = 20$ K from decreasing to growing. Interestingly, our MQCT calculations show similar behavior. Figure 8 demonstrates that at very low temperature the rate coefficient $\kappa_{10}(T)$ starts growing, in contrast to the monotonic decrease, expected from T-dependence in Fig. 7. In fact, one can show this analytically: As $E \to 0$ we have $U \to \Delta\varepsilon/4$ and, at zero-order, we can replace the dependence of $\tilde{\sigma}_{10}(U) \cdot E$ by a constant number proportional to $P_{10}(\Delta\varepsilon/4)$ which corresponds to rotation-less transition at $T = 0$. Then, from Eq. (9) we can obtain the lower boundary estimate

$$\kappa_{10}^{\mathrm{dir}}(T) \geq \sqrt{\frac{8kT}{\mu\pi}} \frac{\pi\hbar^2}{2\mu(kT)^2} P_{10}(\Delta\varepsilon/4) \int_0^\infty \exp\left(-\frac{E}{kT}\right) dE$$

$$= \sqrt{\frac{2\pi\hbar^4}{\mu^3 kT}} P_{10}(\Delta\varepsilon/4). \qquad (28)$$

So, we see that in the $T \to 0$ limit one should expect to observe $\kappa_{10}(T) \to \infty$, and our calculations near $T = 5$ K really show this. Note that this is a classical behavior, different from the quantum mechanical Wigner law that becomes valid at sub-Kelvin temperatures.[56]

As for the absolute value of rate coefficient, the largest discrepancy between the MQCT rate and the full-quantum rate of Balakrishnan[15] is observed near $T = 20$ K. There, our result is about a factor of $\times 4$ higher, which can probably be judged as semi-quantitative agreement. Note that at $T < 100\,K$ we did not try to reach convergence and run only few hundred trajectories to obtain an estimate of cross section (20% –30% statistical error). Also, like Balakrishnan,[15] we included only the values of j up to $j = 3$, in order to make comparison straightforward.

Finally, we computed the values of converged quenching cross sections for a broad range of collision energies. Note that such cross sections are not really needed anywhere in the mixed quantum/classical treatment of kinetics. We did these calculations only in order to conduct a detailed comparison of the MQCT results against results of the full quantum methods. Figure 9 shows our data (green line) in comparison with CC calculations of Balakrishnan[15] (blue symbols), and CS calculations of Krems[17] (red symbols) on the same PES. The

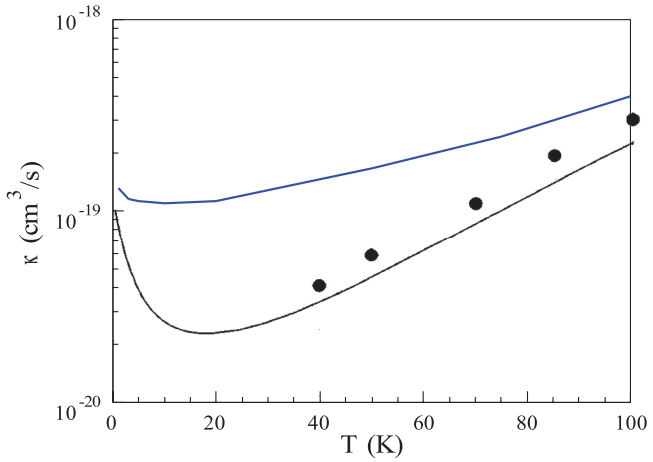

FIG. 8. Rate coefficients for quenching of CO($v = 1$) by He impact in the low temperature range obtained here (blue line) in comparison with full quantum calculations of Ref. 15 (black line) and experimental values from Ref. 53 (symbols).

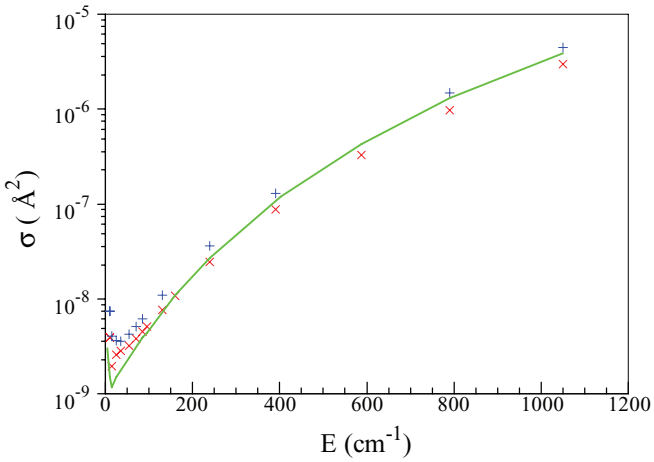

FIG. 9. Cross sections for quenching of CO($v = 1$) by He impact obtained by MQCT method (green line) in comparison with full quantum CC results from Ref. 15 and CS results from Ref. 17 (blue and red symbols, respectively).

overall trend of energy dependence is reproduced really well. At collision energies above 100 cm^{-1}, the MQCT results lie between CC and CS results. At lower energies, the MQCT cross sections are somewhat underestimated (e.g., by a factor of $\times 4$ compared to CC results of Balakrishnan[15] at $E = 10\,cm^{-1}$) and are closer to CS results of Krems.[17] Note, however, that in this energy range there is a discrepancy by about a factor $\times 2$ even between results of two quantum methods. Overall, the agreement of MQCT with full quantum methods can be judged as good.

V. CONCLUSIONS

The mixed quantum/classical approach was applied to the problem of ro-vibrational energy transfer in the inelastic collisions of CO($v = 1$) with He atom, in order to predict the quenching rate coefficient in a broad range of temperatures $5\,K < T < 2500\,K$. Scattering calculations were done in two different ways: (i) direct calculations of quenching cross sections or, alternatively (ii) calculations of excitation cross sections plus microscopic reversibility. At temperatures $T > 500\,K$, the second approach gives quenching rate coefficients in excellent agreement with experiment.

At $T < 500\,K$, the second approach overestimates rate coefficients, but this problem can be easily fixed by forcing the excitation cross section to vanish in the physically irrelevant energy range (below the reaction threshold) and grow smoothly just above the threshold. In contrast, the first approach (direct quenching) underestimates the reaction rate coefficient for CO($v = 1$) + He, but we showed that this problem must be less severe in the molecules and/or processes with smaller vibrational quanta involved (e.g., near the dissociation limit).

Furthermore, the problem at low energies can be easily avoided by using (iii) a symmetrized average-velocity approach of Billing.[45] It gives good agreement with experiment at $T < 500\,K$ using either cross sections for direct quenching, or those for excitation + reversibility. Note that no extra scattering calculations are needed for this third approach: the data used in either (i) or (ii), or both simultaneously, can be utilized. Even at very low temperatures $5 < T < 50\,K$, the agreement of predicted quenching rates with experimental data and with full quantum calculations was within half order of magnitude.

In one statement, we can formulate our overall recommendation as follows: The MQCT calculations of the relaxation rate coefficients should be carried out in the reverse direction (excitation) using the principle of microscopic reversibility; at low collision energies, the symmetrized (average velocity) approach of Billing[45] is essential, but at high collision energies it is not really needed.

It should be emphasized that the CO($v = 1$) + He system studied here represents a stringent test of the MQCT method. First, the vibrational quantum in CO is rather large and, second, the He quencher is very light. For heavier quenchers and closer to dissociation limit of the molecule, the MQCT method is expected to work even better.

ACKNOWLEDGMENTS

Professor Balakrishnan Naduvalath at UNLV is gratefully acknowledged for stimulating discussions. This research was supported by NSF, partially through Atmospheric Chemistry Program, Grant No. 1252486, and partially through Theoretical Chemistry Program, Grant No. 1012075. This research used resources of the National Energy Research Scientific Computing Center, which is supported by the Office of Science of the (U.S.) Department of Energy (DOE) under Contract No. DE-AC02-05CH11231.

APPENDIX: QUENCHING RATE COEFFICIENT EXPRESSED THROUGH CROSS SECTION FOR EXCITATION

First, consider the numerator of Eq. (8)

$$\sum_{j'}\sum_{j}(2j+1)\exp\left(-\frac{\varepsilon_1^j}{kT}\right)\int_0^\infty \sigma_{10}^{jj'}(E)E\exp\left(-\frac{E}{kT}\right)dE, \tag{A1}$$

and move the integral sign outside of the double-sum. Then rearrange the order of factors as follows:

$$\int_0^\infty \sum_{j'}\sum_{j}(2j+1)\sigma_{10}^{jj'}(E)E\exp\left(-\frac{E+\varepsilon_1^j}{kT}\right)dE. \tag{A2}$$

This version allows using Eqs. (13) and (14) straight in order to replace the pre-exponential factor and the numerator of the exponent, respectively. These substitutions give

$$\int_{\Delta\varepsilon}^\infty \sum_{j'}\sum_{j}(2j'+1)\sigma_{01}^{j'j}(E')E'\exp\left(-\frac{E'+\varepsilon_0^{j'}}{kT}\right)dE'. \tag{A3}$$

Note also that we have changed the variable of integration and the limits of integration. Indeed, based on Eq. (14), for integration over the collision energy of each individual state-to-state transition we have $dE = dE'$and we also see that $E' = \varepsilon_1^j - \varepsilon_0^{j'} \approx \Delta\varepsilon$ when $E = 0$. The latter approximation is based on the fact that rotational quantum of energy is much smaller than vibrational quantum. One can easily avoid this approximation, but then each term of the double-sum in Eq. (A3) will have its own specific lower limit of integration. This is inconvenient, and for simplicity we use $\Delta\varepsilon \approx \varepsilon_1^j - \varepsilon_0^{j'}$.

Now consider denominator of Eq. (8). It represents the rotational partition function of the excited vibrational state $v = 1$

$$Q_1 = \sum_j (2j+1)\exp\left(-\frac{\varepsilon_1^j}{kT}\right). \tag{A4}$$

Introducing similar partition function for the ground vibrational state, Q_0, and formally replacing Q_1 in the denominator of Eq. (8) by $Q_0 \times (Q_1/Q_0)$, we obtain the following

expression:

$$\kappa_{10}^{\text{rev}}(T) = \frac{Q_0}{Q_1}\sqrt{\frac{8kT}{\mu\pi}}\frac{1}{(kT)^2}\int_{\Delta\varepsilon}^{\infty}\tilde{\sigma}_{01}(E')E'\exp\left(-\frac{E'}{kT}\right)dE'. \tag{A5}$$

Here, by analogy with Eq. (10), we introduced the rotationally averaged cross section for the reverse vibrational transition (excitation)

$$\tilde{\sigma}_{01}(E') = \frac{\sum_j\sum_{j'}(2j'+1)\exp\left(-\frac{\varepsilon_0^{j'}}{kT}\right)\sigma_{01}^{j'j}(E')}{\sum_{j'}(2j'+1)\exp\left(-\frac{\varepsilon_0^{j'}}{kT}\right)}. \tag{A6}$$

Also, by analogy with Eq. (9), we can define rate coefficient for the reverse transition (excitation) as

$$\kappa_{01}(T) = \sqrt{\frac{8kT}{\mu\pi}}\frac{1}{(kT)^2}\int_{\Delta\varepsilon}^{\infty}\tilde{\sigma}_{01}(E')E'\exp\left(-\frac{E'}{kT}\right)dE'. \tag{A7}$$

Note, however, that integration in Eq. (A7) starts at $E' = \Delta\varepsilon$, different from Eq. (9), where integration starts at $E = 0$. This makes physical sense because if we start from $v' = 0$ the channel $v = 1$ is open only when the collision energy E' exceeds the excitation energy ($E' \geq \Delta\varepsilon$), while if we start from $v = 1$ the channel $v' = 0$ is open at any collision energy ($E \geq 0$). Formally, one could expand the limits of integration in Eq. (A7) down to $E' = 0$, but only if the excitation cross section $\tilde{\sigma}_{01}(E')$ exhibits the correct property: $\tilde{\sigma}_{01} = 0$ when $E' < \Delta\varepsilon$. In any case, using Eq. (A7) in Eq. (A5), we obtain

$$\kappa_{10}Q_1 = \kappa_{01}Q_0, \tag{A8}$$

which is a thermally averaged (canonical) analogue of the micro-canonical expression of Eq. (13).

Now take a look at the ratio Q_0/Q_1 in Eq. (A5). Each of Q_0 and Q_1 can be written as a product of rotational partition function and vibrational factor. For the low lying vibrational states, the rotational partition functions are approximately equal and they approximately cancel in the Q_0/Q_1 ratio. Only the ratio of vibrational factors survives and gives

$$\frac{Q_0}{Q_1} = \frac{\sum_{j'}(2j'+1)\exp\left(-\frac{\varepsilon_0^{j'}}{kT}\right)}{\sum_j(2j+1)\exp\left(-\frac{\varepsilon_1^{j}}{kT}\right)} \approx \exp\left(\frac{\Delta\varepsilon}{kT}\right). \tag{A9}$$

This term can be brought inside the integral in Eq. (A5), which gives

$$\kappa_{10}^{\text{rev}}(T) \approx \sqrt{\frac{8kT}{\mu\pi}}\frac{1}{(kT)^2}\int_{\Delta\varepsilon}^{\infty}\tilde{\sigma}_{01}(E')E'\exp\left(-\frac{E'-\Delta\varepsilon}{kT}\right)dE'. \tag{A10}$$

Expression (A10) suggests to change the integration variable back to $E = E' - \Delta\varepsilon$, which finally leads to

$$\kappa_{10}^{\text{rev}}(T) \approx \sqrt{\frac{8kT}{\mu\pi}}\frac{1}{(kT)^2} \times \int_0^{\infty}\tilde{\sigma}_{01}(E+\Delta\varepsilon)(E+\Delta\varepsilon)\exp\left(-\frac{E}{kT}\right)dE. \tag{A11}$$

So, this expression is approximate. In order to make it look similar to Eq. (9) we, first, introduced a single lower integration limit $\Delta\varepsilon \approx \varepsilon_1^j - \varepsilon_0^{j'}$ in Eq. (A3) and, second, neglected the ratio of rotational partition functions in Eq. (A9). The exact (much bulkier) version of Eq. (A11) can be easily recovered, if needed.

[1] J. C. Stephenson and E. R. Mosburg, Jr., J. Chem. Phys. **60**, 3562 (1974).
[2] G. Quéméner and N. Balakrishnan, Phys. Rev. A **77**, 030704(R) (2008).
[3] W. H. Green and J. K. Hancock, J. Chem. Phys. **59**, 4326 (1973).
[4] R. C. Millikan, J. Chem. Phys. **40**, 2594 (1964).
[5] D. J. Miller and R. C. Millikan, J. Chem. Phys. **53**, 3384 (1970).
[6] Y. B. Band and P. S. Julienne, Phys. Rev. A **51**, R4317 (1995).
[7] A. Fioretti, D. Comparat, A. Crubellier, O. Dulieu, F. Masnou-Seeuws, and P. Pillet, Phys. Rev. Lett. **80**, 4402 (1998).
[8] F. A. Gianturco, F. Paesani, M. F. Laranjeira, V. Vassilenko, M. A. Cunha, A. G. Shashkov, and A. F. Zolotukhina, Mol. Phys. **94**, 605 (1998).
[9] E. Bodo, F. A. Gianturco, and F. Paesani, Z. Phys. Chem. (Leipzig) **214**, 1013 (2000).
[10] F. A. Gianturco, N. Sanna, and S. Serna, J. Chem. Phys. **98**, 3833 (1993).
[11] R. Kobayashi, R. D. Amos, J. P. Reid, H. M. Quiney, and C. J. S. M. Simpson, Mol. Phys. **98**, 1995 (2000).
[12] S. Antonova, A. Lin, A. P. Tsakotellis, and G. C. McBane, J. Chem. Phys. **110**, 2384 (1999).
[13] J. P. Reid, C. J. S. M. Simpson, H. M. Quiney, and J. M. Hutson, J. Chem. Phys. **103**, 2528 (1995).
[14] J. P. Reid, C. J. S. M. Simpson, and H. M. Quiney, J. Chem. Phys. **107**, 9929 (1997).
[15] N. Balakrishnan, A. Dalgarno, and R. C. Forrey, J. Chem. Phys. **113**, 621 (2000).
[16] R. V. Krems, J. Chem. Phys. **116**, 4517 (2002).
[17] R. V. Krems, J. Chem. Phys. **116**, 4525 (2002).
[18] C. T. Wickham-Jones, H. T. Williams, and C. J. S. M. Simpson, J. Chem. Phys. **87**, 5294 (1987).
[19] C. Cecchi-Pestellini, E. Bodo, N. Balakrishnan, and A. Dalgarno, Astrophys. J. **571**, 1015 (2002).
[20] H. Uitenbroek, Astrophys. J. **536**, 481 (2000).
[21] A. Evans, T. R. Geballe, J. M. C. Rawlings, and A. D. Scott, Mon. Not. R. Astron. Soc. **282**, 1049 (1996).
[22] W. Liu and A. Dalgarno, Astrophys. J. **454**, 472 (1995).
[23] P. Saxena and F. A. Williams, Combust. Flame **145**, 316 (2006).
[24] J. B. Howard, G. C. Williams, and D. H. Fine, Sym. (Int.) Combust., [Proc.] **14**, 975 (1973).
[25] N. Balakrishnan and G. D. Billing, J. Chem. Phys. **104**, 9482 (1996).
[26] H. L. Bethlem, G. Berden, and G. Meijer, Phys. Rev. Lett. **83**, 1558 (1999).
[27] J. A. Maddi, T. P. Dinneen, and H. Gould, Phys. Rev. A **60**, 3882 (1999).
[28] M. Thachuk, C. E. Chuaqui, and R. J. Le Roy, J. Chem. Phys. **105**, 4005 (1996).
[29] F. A. Gianturco, F. Paesani, M. F. Laranjeira, V. Vassilenko, M. A. Cunha, A. G. Shashkov, and A. F. Zolotoukhina, Mol. Phys. **92**, 957 (1997).
[30] M.-C. Chan and A. R. W. McKellar, J. Chem. Phys. **105**, 7910 (1996).
[31] R. Moszynski, T. Korona, P. E. S. Wormer, and A. van der Avoird, J. Chem. Phys. **103**, 321 (1995).
[32] F.-M. Tao, S. Drucker, R. C. Cohen, and W. Klemperer, J. Chem. Phys. **101**, 8680 (1994).
[33] B. Kukawska-Tarnawska, G. Chalasinski, and K. Olszewski, J. Chem. Phys. **101**, 4964 (1994).
[34] T. G. A. Heijmen, R. Moszynski, P. E. S. Wormer, and A. van der Avoird, J. Chem. Phys. **107**, 9921 (1997).

[35]K. A. Peterson and G. C. McBane, J. Chem. Phys. **123**, 084314 (2005).
[36]N. Balakrishnan, V. Kharchenko, and A. Dalgarno, J. Geophys. Res. **103**, 23393, doi:10.1029/98JA02198 (1998).
[37]W. H. Miller, W. L. Hase, and C. L. Darling, J. Chem. Phys. **91**, 2863 (1989).
[38]G. D. Billing, Comput. Phys. Rep. **1**, 239 (1984).
[39]M. Ivanov and D. Babikov, J. Chem. Phys. **134**, 144107 (2011).
[40]M. Ivanov and D. Babikov, J. Chem. Phys. **134**, 174308 (2011).
[41]M. Ivanov and D. Babikov, J. Chem. Phys. **136**, 184304 (2012).
[42]M. Ivanov and D. Babikov, "On molecular origin of mass-independent fractionation of oxygen isotopes in the ozone forming recombination reaction," Proc. Natl. Acad. Sci. U.S.A. (published online).
[43]D. Babikov, R. B. Walker, and R. T. Pack, J. Chem. Phys. **117**, 8613 (2002).
[44]R. T. Pack, R. B. Walker, and B. K. Kendrick, J. Chem. Phys. **109**, 6714 (1998).
[45]G. D. Billing, *The Quantum-Classical Theory* (Oxford University Press, 2003).
[46]A. Semenov and D. Babikov, J. Chem. Phys. **138**, 164110 (2013).
[47]C. Leforestier, R. H. Bisseling, C. Cerjan, M. D. Feit, R. Friesner, A. Guldberg, A. Hammerich, G. Jolicard, W. Karrein, H.-D. Meyer, N. Lipkin, O. Roncero, and R. Kosloff, J. Comput. Phys. **94**, 59 (1991).
[48]G. Billing, J. Chem. Phys. **99**, 5849 (1993).
[49]R. K. Preston and R. T. Pack, J. Chem. Phys. **66**, 2480 (1977).
[50]W. H. Press, B. P. Flannery, S. A. Teukolsky, and W. T. Vetterling, *Numerical Recipes* (Cambridge University Press, 1989).
[51]T. J. Park and J. C. Light, J. Chem. Phys. **85**, 5870 (1986).
[52]G. S. Whittier and J. C. Light, J. Chem. Phys. **110**, 4280 (1999).
[53]G. J. Wilson, M. L. Turnidge, A. S. Solodukhin, and C. J. S. M. Simpson, Chem. Phys. Lett. **207**, 521 (1993).
[54]J. C. Tully, J. Chem. Phys. **93**, 1061 (1990).
[55]R. D. Levine, *Quantum Mechanics of Molecular Rate Processes* (Clarendon, Oxford, 1969).
[56]E. P. Wigner, Phys. Rev. **73**, 1002 (1948).